Available online at www.sciencedirect.com
SCIENCE DIRECT®
Journal of Structural Biology 151 (2005) 306–314
Journal of Structural Biology
www.elsevier.com/locate/yjsbi

The 17 Å structure of the 420 kDa lobster clottable protein by single particle reconstruction from cryoelectron micrographs

Justin M. Kollman [a,*], Joel Quispe [b]

[a] *Division of Biological Sciences, University of California, San Diego, La Jolla, CA 92093-0314, USA*
[b] *Department of Cell Biology, The Scripps Research Institute, La Jolla, CA 92037, USA*

Received 12 April 2005; received in revised form 9 June 2005; accepted 13 June 2005
Available online 15 August 2005

Abstract

Crustaceans form clots by the rapid crosslinking of a hemolymph clottable protein (CP) to form long, branched polymers. Clotting limits hemolymph loss from wounds as well as playing a part in the innate immune response. CP is a 420 kDa homodimer with a large quantity of associated lipid, primarily the carotenoid pigment astaxanthin. The three-dimensional structure of CP from the lobster *Panulirus interruptus* has been determined to 17 Å resolution by single particle reconstruction from electron micrographs of the protein embedded in vitreous ice. The most prominent feature of this structure is a large cavity spanning the length of the molecule, which is the likely lipid binding pocket. The EM structure has been used in a low resolution molecular replacement search with data from orthorhombic CP crystals, and a solution is presented which describes the crystal packing.

Keywords: Clotting; Lipid binding; Single particle reconstruction; Cryoelectron microscopy

1. Introduction

The ability to form blood clots has evolved independently in various animal phyla. Although the mechanisms of formation differ greatly, animals as diverse as vertebrates, insects, echinoderms, and crustaceans all form insoluble plugs in response to wounds. In many invertebrates clotting is also part of an innate immune response, serving to immobilize pathogens prior to their destruction by melanization (Soderhall and Cerenius, 1998).

In decapodal crustaceans, clotting consists of the polymerization of a large circulating clottable protein (CP) into long, branched chains which form a gel. The polymerization is mediated by a transglutaminase released from hemocytes upon injury, which catalyzes the formation of isopeptide linkages between one or more lysine sidechains of one CP molecule and one or more glutamine sidechains of another CP molecule (Fuller and Doolittle, 1971b; Kopacek et al., 1993).

In the California spiny lobster, *Panulirus interruptus*, the clottable protein is a glycosylated 420 kDa homodimer. Approximately 5% of the molecule's mass is acetone-extractable lipid, the predominant component of which is astxanthin, a carotenoid pigment also found in the shell and eggs of the lobster (Fuller and Doolittle, 1971a). CP is homologous to vitellogenin, a lipid transport protein deposited in eggs to provide nourishment to developing embryos (Doolittle and Riley, 1990; Hall et al., 1999; Yeh et al., 1999). Vitellogenin and CP belong to a larger family of lipid-binding proteins which include insect apolipophorin II/I and vertebrate apolipoprotein B (Babin et al., 1999).

The structure of vitellogenin from lamprey has been determined by X-ray crystallography (Raag et al., 1988), and models of apolipoprotein B and apolipophorin II/I

* Corresponding author.
E-mail address: jkollman@biomail.ucsd.edu (J.M. Kollman).

1047-8477/$ - see front matter © 2005 Elsevier Inc. All rights reserved.
doi:10.1016/j.jsb.2005.06.008

have been built based on this structure (Richardson et al., 2005; Smolenaars et al., 2005). In these models, the more conserved amino-terminal 600 residues form a β-barrel domain and a coiled, horsehoe-shaped α-helical domain. The less conserved carboxy-terminal portions of these molecules consist mostly of two or three amphipathic β sheets, the hydrophobic surfaces of which form a large lipid-binding cavity. There is a conserved vonWillebrand D domain at the carboxy terminus of most of these lipoproteins which may be involved in oligomerization, but which was not present in the lamprey crystal structure.

There is reason to believe that the clottablity of CP evolved by the insertion of an approximately 30-residue sequence into a surface loop of the conserved amino-terminal β-barrel domain. The insert is found exclusively in the two known CP sequences and consists primarily of Ser-Lys-Thr-Ser repeats, suggestive of a hydrophilic, disordered loop. The lysine residues within this region are the proposed substrates for transglutaminase crosslinking; glutamine-rich regions in the carboxy-terminal half of the molecule are the most likely crosslinking donor sites (Hall et al., 1999; Yeh et al., 1999).

In this report, the structure of lobster CP has been reconstructed from cryo-electron micrographs to a resolution of 17 Å. At this resolution the gross features of the roughly tetrahedral molecule are apparent, the most striking of which is a large central cavity which had not been apparent in micrographs of negatively stained CP (Fuller and Doolittle, 1971b; Hall et al., 1999). We propose that this cavity constitutes a lipid binding pocket, similar to that of vitellogenin.

The current study was undertaken in the wake of X-ray diffraction experiments with CP crystals. Although CP crystals diffract to a maximum resolution of 3.2 Å, attempts to phase the data by the conventional means of molecular replacement with the homologous lamprey vitellogenin structure or by heavy atom derivatization have been unsuccessful (Kollman and Doolittle, 2005). The hope was that an EM structure could be used to generate low resolution phases for the crystal data, as the initial step in determining the crystal structure. To that end, a molecular envelope search has been used to position the EM model in the unit cell of the CP crystal.

2. Materials and methods

2.1. Sample preparation

The purification of clottable protein from lobster hemolymph has been described elsewhere (Kollman and Doolittle, 2005). For negative stain experiments, purified protein was diluted to 100 μg/ml in water, applied to 400 mesh copper grids with carbon support film and stained with Nano-W (Nanoprobes). For cryo-EM experiments, purified protein was diluted to 1 mg/ml and applied to Quantifoil grids (Quantifoil Micro Tools, GmbH). The grids were blotted for 3.5 s and frozen using a Vitrobot (FEI) automated vitrification device.

2.2. Electron microscopy

Three data sets were collected (Table 1): a negative stain data set, a high dose cryo data set from which an initial model was generated, and a large cryo reconstruction data set.

The grids were inserted into a Phillips Tecnai F20 electron microscope set to an accelerating voltage of 120 kV. Images were recorded on a Teitz SCX 4096 × 4096 pixel slow-scan CCD detector. The *Leginon* software system was used for automated data collection (Carragher et al., 2000; Potter et al., 1999). *Leginon* acquires images of the grid at increasing magnification scales, allowing for target selection at each step. The starting point is the creation of an overall atlas of the grid at 120× magnification. Targets were selected on the atlas for imaging of individual grid squares (550×). In cryo experiments holes in the carbon support film of suitable ice thickness were selected and imaged (5000×) and a final target selection identified regions within these holes for high magnification particle imaging (50,000×). High magnification focus images were also taken of an area of carbon support film outside of each hole. In negative stain experiments, targets at 5000× and 50,000× magnification were selected in a simple grid on the lower magnification image. The defocus settings and electron doses of the various data sets are summarized in Table 1. Micrographs of the reconstruction data set were acquired in focal pairs, with the further from focus images used only for selecting particles.

Table 1
Electron microscopy data sets

Data set	Micrographs	Particles	Defocus setting		Average dose ($e^-/Å^2$)
			Particle images (μm)	Focus images (μm)	
Negative stain	441	6916	−1	n/a[a]	10
Initial model	63	4709	−3	−2	30
Reconstruction	430	19083	−1.5 /−3.0[b]	−2	10

[a] Defocus was measured directly from negative stain micrographs.
[b] Micrographs were acquired in focal pairs, with the −3.0 μm images used for particle selection.

Promising grid squares were manually selected from the atlas, but at all subsequent steps the targets were determined by the software system. The automated system allowed for a maximum of 25 high magnification focal pairs—with corresponding images of grid squares and holes—to be collected per hour. The images acquired at high magnification were at a pixel size of 1.63 Å/pixel.

2.3. Three-dimensional reconstruction

The reconstruction was performed using programs of the *EMAN* software suite (Ludtke et al., 1999). For the negative stain and initial model data sets, particles were manually selected from the micrographs using the *EMAN* program *boxer*. Focal pairs of the reconstruction data set were aligned with the program *Selexon* (Zhu et al., 2004). Particles were then manually selected on the further from focus images and extracted from the nearer to focus micrographs for use in the reconstruction.

The *Suprim* software suite (Schroeter and Bretaudiere, 1996) was used to measure the defocus from the power spectra of focus images taken over the carbon film. The defocus value of each particle image was then calculated by applying the offset between the defocus settings of that image and the corresponding focus image. For all data sets, rotationally averaged power spectra were calculated from the boxed out particles from each micrograph with the *EMAN* program *ctfit*. The defocus of negative stain particles could be measured directly in *ctfit*. For all images contrast transfer function (CTF) noise parameters were manually adjusted to fit the power spectra, the individual images were phase-flipped, and the CTF parameters were stored for use in CTF correction during reconstruction.

The reconstruction from negative stain particles began with a model generated from reference-free class averages aligned by the cross common lines method with the *EMAN* programs *startnrclasses* and *startAny*. Eight rounds of iterative projection matching and model building were carried out on particle images low pass filtered at 25 Å. The two halves of the CP dimer are related by a twofold rotational axis (Kollman and Doolittle, 2005); C2 point group symmetry was therefore imposed throughout the reconstruction. The final negative stain model was low pass filtered at 35 Å using the *EMAN* program *proc3d*.

The initial model data set was used to generate reference-free class averages and a cross common lines model by the same technique used with the negative stain data above. Beginning with this initial model, forty rounds of iterative projection matching and model building were carried out with the reconstruction data set. The images were low pass filtered at 25 Å for the first 10 rounds, at 15 Å for the following 10 rounds, and at 5 Å for the final 20 rounds. A 9° increment was used in generating model projections, C2 point group symmetry was imposed, and CTF correction was implemented using the *ctfc* flag of the *refine* command. The *classkeep* flag was set to 0.5 throughout, which caused particles which poorly matched their class averages to be excluded in each round of reconstruction.

The resolution of the model was monitored with the *eotest* command of *EMAN*, which randomly splits the data set into two groups for separate reconstructions and compares the resulting models by the Fourier shell correlation (FSC) technique (Saxton and Baumeister, 1982; Van Heel, 1987). The resolution of the model was defined to be the spatial frequency at which the FSC dropped to 0.5. A parallel reconstruction was also performed by the same procedure, but with density from the negative stain reconstruction used as the initial model for classifying the cryo images. The volumes resulting from the parallel reconstructions were manually aligned and compared to each other by the FSC method.

Models were low pass filtered at the resolution suggested by the FSC test using the *EMAN* program *proc3d*, and set with the program *volume* so that a threshold of 1.0 incorporated the expected 420 kDa mass of the CP dimer. Chimera (Pettersen et al., 2004) was used to view the models, and *O* (Jones et al., 1991) was used in attempts to fit conserved domains into the final structure and for positioning astaxanthin molecules into the central cavity.

2.4. Crystal data collection

Crystals of lobster CP were grown and prepared for X-ray diffraction experiments as described (Kollman and Doolittle, 2005). A low resolution data set was collected on a rotating copper anode X-ray source with a MAR345 image plate (marUSA), care being taken to obtain accurate measurements of very low resolution reflections by avoiding saturation. The data were indexed, integrated and scaled with the HKL software package (Otwinowski and Minor, 1997). Data collection statistics are summarized in Table 2.

Table 2
Crystal data collection statistics

Values in parentheses are for the highest resolution shell	
Spacegroup	$P2_12_12_1$
Unit cell dimensions	$a = 120.9$
	$b = 183.6$
	$c = 186.0$
	$\alpha = \beta = \gamma = 90°$
Resolution	50–10 Å
Completeness	100 (100) %
R_{merge}[a]	0.064 (0.087)
Total reflections	24,195
Unique reflections	2448
Mosaicity	0.38°

[a] $R_{merge} = \Sigma_{hkl}\Sigma_i |I_i(hkl) - \langle I(hkl)\rangle| / \Sigma_{hkl}\Sigma_i I_i(h\,kl)$.

2.5. Molecular replacement

Real-space molecular envelope searches were performed with the program *FSEARCH*, which simultaneously searches both rotation and translation of the model (Liu et al., 2003). The noncrystallographic twofold symmetry axis had previously been located by the self rotation in orthorhombic crystals at the Eulerian angles $\alpha = 90°$, $\beta = 45°$. By positioning the dimeric twofold axis of the EM model parallel to the observed noncrystallographic twofold the initial search was reduced to a single rotation (γ) about that axis and three translational vectors. Several searches were carried out with each enantiamorph of the EM model, scaled between 0.95 and 1.05 times its original size. Each search was repeated using data in various resolution ranges. The translational vectors were searched on a $126 \times 190 \times 190$ grid. The initial searches were done at 3° intervals about γ and four grid units in each dimension. Finer, six-dimensional searches were performed in restricted regions around promising results from the four-dimensional searches at 1° intervals in α, β, and γ and two grid units in each dimension. The final solution was checked for overlap with symmetry mates using the chkoverlap flag of *FSEARCH*.

3. Results

A three-dimensional model of the lobster clottable protein (CP) was determined by single particle reconstruction from cryoelectron micrographs. The projections of CP in negative stain and cryo images varied in diameter from 8 to 12 nm, and were predominantly triangular or diamond-shaped, as has been observed previously (Fuller and Doolittle, 1971b; Hall et al., 1999). Unlike negatively stained samples, however, many projections of CP dimers frozen in ice had large central cavities (Fig. 1).

A preliminary reconstruction from negatively stained particles at low resolution was carried out to determine the feasibility of performing a three-dimensional reconstruction on the relatively small CP dimer. The results of this reconstruction (not shown) encouraged the reconstruction from cryoelectron micrographs.

The size of CP dimers combined with a relatively low defocus setting (−1.5 μm) resulted in images with extremely low contrast between particles and the surrounding ice (Fig. 1C). This presented two difficulties in the three-dimensional reconstruction, the first of which was generating an accurate model for the first round of projection matching. The initial model was constructed using the cross common lines approach with reference-free class averages (Ludtke et al., 1999). Models made with reference-free class averages of the reconstruction data set vary greatly depending on the number of particles used. To obtain a more accurate low resolution starting model, a set of images was collected at a higher electron dose (30 $e^-/Å^2$). The resulting 4709 particle images provided higher contrast and generated clearer reference-free class averages. The initial model derived from this data set, though lacking higher resolution features, appeared to more accurately reflect the general shape of the molecule (Fig. 2). This model has the triangular and diamond-shaped aspects seen in both negative stain and cryoelectron micrographs

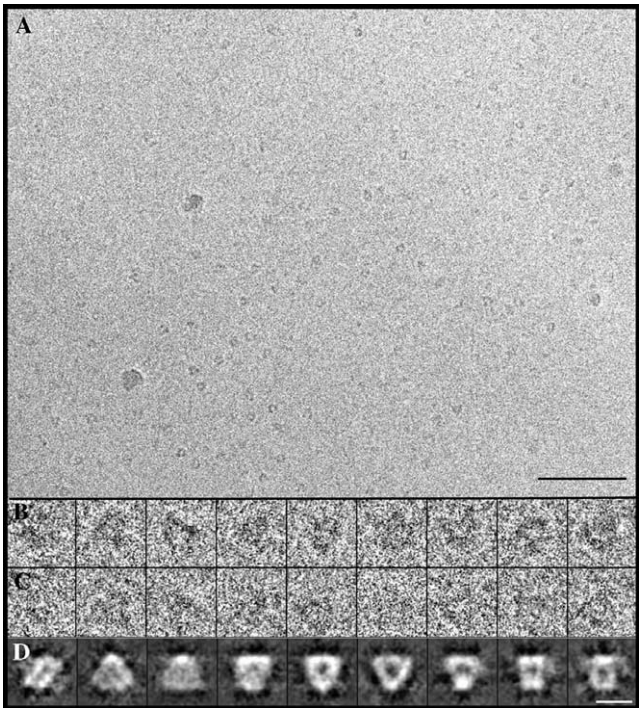

Fig. 1. (A) Section of a micrograph of lobster clottable protein frozen in vitreous ice, taken at −3 μm defocus. Scalebar, 100 nm. (B) Sample of particles selected from −3μm micrographs and (C) their focal pairs from −1.5μm images. (D) Class averages from the final reconstruction round demonstrating the twofold symmetry relating the halves of the CP dimer. The class average at left is the projection down the twofold axis, while the remaining projections are perpendicular to the twofold axis. Scale bar for (B, C, and D), 10 nm.

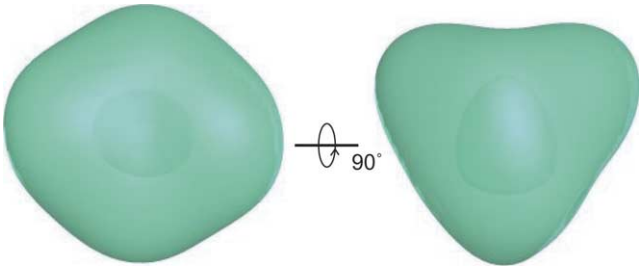

Fig. 2. Initial model for reconstruction. Reference-free class averages were generated from particles of high dose, −3.0 μm defocus cryoelectron micrographs. The averages were aligned by cross common lines and a model generated with C2 symmetry imposed. The density is rendered slightly transparent to show the central cavity.

(Fuller and Doolittle, 1971b; Hall et al., 1999), as well as the central cavity seen in the cryo images. Moreover, projections of this model more closely resemble the individual particles from the micrographs.

The second difficulty was in accurately classifying and aligning defocus particles of the reconstruction data set due to high noise. The strategy which gave the best reconstruction results was to low pass filter the particles at increasingly high resolution in successive iterations. The data were low pass filtered at 25 Å in the first 10 rounds of refinement, followed by 10 rounds with data low pass filtered at 15 Å, and finally 20 rounds with data low pass filtered at 5 Å.

A total of 19,083 particles were selected from micrographs, of which 15,474 were incorporated into the model in the final round of reconstruction; the remaining particles were excluded on the basis of poorly matching their corresponding class averages. The class averages corresponding to the view down the imposed symmetry axis and perpendicular to that axis (Fig. 1D) confirm the twofold rotational relationship between the CP monomers that has been described in crystallographic studies of the molecule (Kollman and Doolittle, 2005). The particle distribution for the final model is fairly uniform, with a slight under-representation of projections perpendicular to the twofold symmetry axis (Fig. 3A). The resolution of the final model, as measured by the spatial frequency at which the FSC drops below 0.5, is 17 Å (Fig. 3B).

The overall shape of the clotting protein is roughly tetrahedral (Fig. 4). The most striking feature of the structure is a large central cavity of roughly 75 nm^3 spanning the width of the molecule. While the reconstruction process does not distinguish between the two possible enantiomorphs, the results of molecular replacement searches indicate that the model shown in Fig. 4 is the correct hand (see below). Attempts were made to position the conserved amino-terminal domains from the structure of lamprey vitellogenin into the reconstructed volume but, given the resolution of the model, it proved impossible to locate these domains unambiguously.

As a control for model bias, a parallel reconstruction was carried out as described above using a reconstruction from negatively stained micrographs as the starting point. The negative stain model had a similar tetrahedral shape, but lacked the central cavity. The two final models are similar, with the FSC between the two dropping to 0.5 at 26 Å. When images low pass filtered at 5 Å were used from the beginning of the reconstruction the 0.5 FSC between the two final models was less than 40 Å, indicating that removing high resolution information from the images in the initial reconstruction rounds was necessary for model convergence.

The final reconstruction was used in a real-space molecular envelope search at low resolution. Previously collected high resolution crystal data (Kollman and Doolittle, 2005) proved unsuitable for these molecular replacement searches because a number of low resolution reflections were saturated. Therefore, a data set was collected with brief exposure to X-rays which resulted in more accurate low resolution data (Table 2). In the envelope searches, three translational vectors and the rotation about the noncrystallographic twofold axis were searched simultaneously. The solution with the lowest *R*-factor and the greatest difference between the top two peaks was found with data from 50 to 25 Å and the enantiomorph pictured in Fig. 4 on the original scale. A finer six-dimensional search in the region surrounding the initial solution resulted in the *R*-factor dropping from 0.547 to 0.512 (Table 3). The overlap between symmetry mates with this solution is only 1.5% of the asymmetric unit volume,

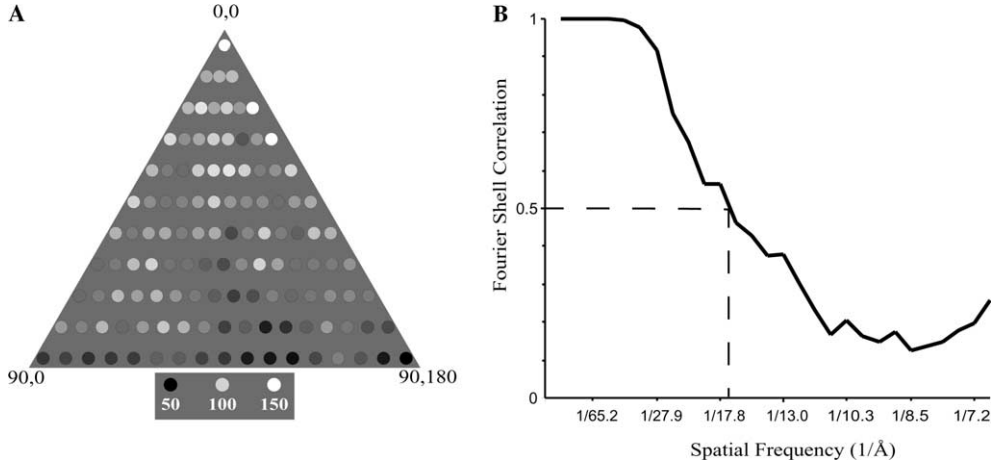

Fig. 3. (A) Distribution of particles into classes. Each circle represents a projection, and the intensity indicates the number of particles in that class. The apex of the triangle corresponds to the projection down the twofold symmetry axis, and the base of the triangle to projections perpendicular to that axis. (B) Estimation of model resolution by the Fourier shell correlation (FSC) method. Two models were constructed, each from one half the data set, and their Fourier transforms compared. The model resolution is taken to be the spatial frequency at which the correlation drops below 0.5.

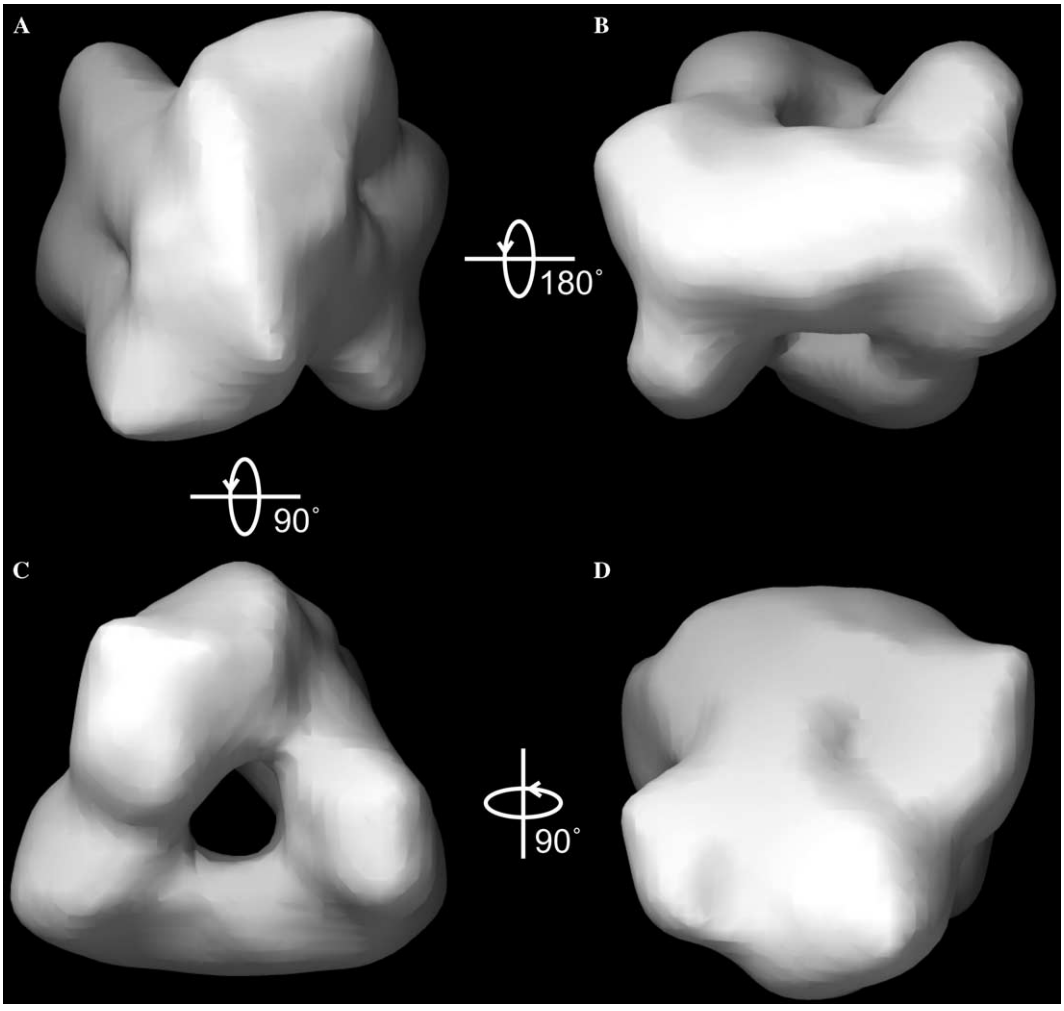

Fig. 4. Surface representation of the three-dimensional reconstruction, low pass filtered at 17 Å and thresholded to include the expected molecular mass of 420 kDa. The views on top are along the dimeric twofold axis, and those on bottom perpendicular to that axis. Arrows indicate the rotational relationships between different views. This and subsequent figures were prepared with Chimera (Pettersen et al., 2004).

Table 3
Molecular envelope search

α (°)	β (°)	γ (°)	X	Y	Z	R
(A) Initial four-dimensional search results						
90	45	126	52	76	40	0.547
90	45	123	56	12	40	0.561
90	45	126	48	36	40	0.563
90	45	123	56	16	40	0.563
90	45	126	48	76	40	0.567
(B) Six-dimensional search around initial peak						
91	45	123	56	76	42	0.512
91	45	123	58	78	42	0.518
91	45	123	58	76	42	0.519
91	45	123	56	78	42	0.521
90	45	124	54	78	40	0.524

The reconstructed EM density was used as the model to simultaneously search rotations about the dimeric axis and translation vectors with the program *FSEARCH* (A top five solutions). A full six-dimensional search limited to the region about the top solution from the initial search yielded a significant drop in the *R*-factor (B top five solutions). Both searches used the data from 50 to 25 Å on a 126 × 190 × 190 grid. *X*, *Y*, and *Z* coordinates are reported as grid units.

which is encouraging in that *FSEARCH* does not take crystal packing into account during the search procedure (Fig. 5). The volume from the negative stain reconstruction and the initial cryo model (Fig. 2) were also used as models for the molecular envelope search. Neither of these models gave solutions with *R*-factors less than 0.6.

4. Discussion

The three-dimensional structure of a crustacean clottable protein (CP) has been determined at a resolution of 17 Å by reconstruction from cryoelectron micrographs of 15,474 individual particles embedded in vitreous ice. The EM structure has been positioned in the unit cell of orthorhombic CP crystals by a low resolution molecular envelope search as a preliminary step toward phasing X-ray diffraction data.

The CP dimer is roughly tetrahedral, with four triangular faces (Figs. 4C and D) and two ridges running

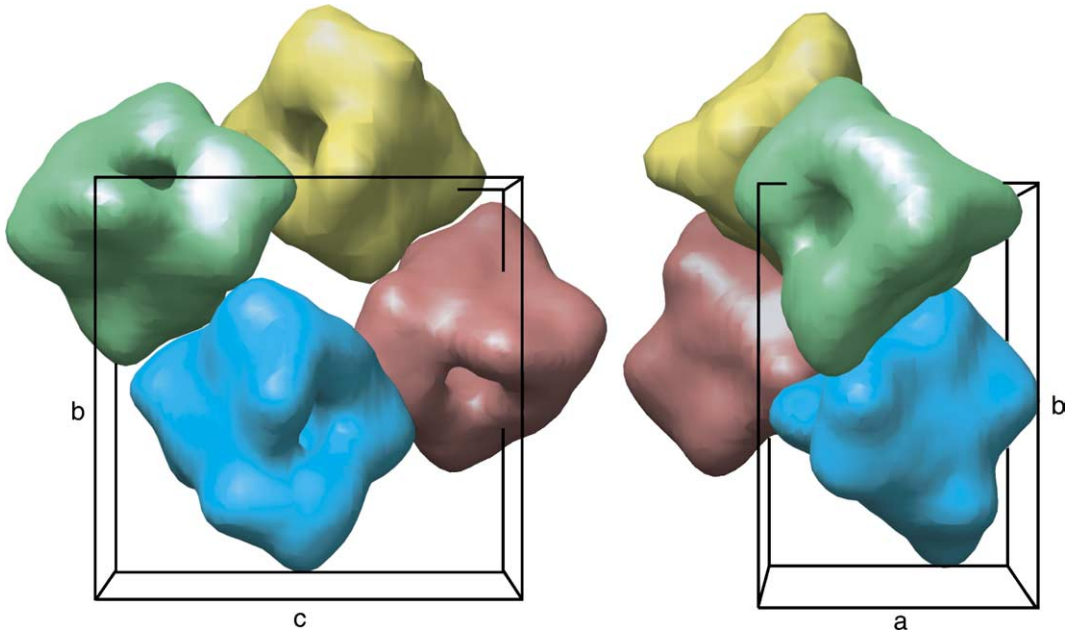

Fig. 5. Packing of the EM density in the CP crystal unit cell. The molecular replacement solution was found with *FSEARCH*, using data to 25 Å (Table 3). The total overlap between molecules is 1.5% of the asymmetric unit volume.

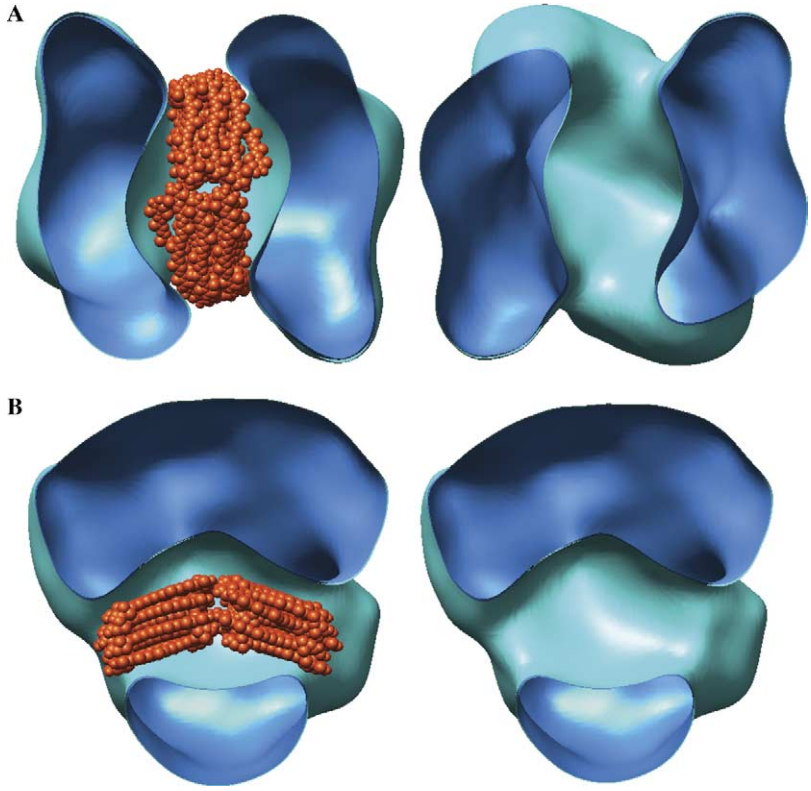

Fig. 6. Cutaway representation of the lipid binding cavity. The surfaces are positioned as in Fig. 4A (A) and Fig. 4D (B). They have been cut in half in the plane of the paper, and opened with the top half on the right. Interior surfaces are rendered in a darker shade. On the left 26 astaxanthin molecules (orange) have been modeled in the cavity.

along opposite sides at roughly right angles to each other (Figs. 4A and B). The dominant feature of the newly determined structure is a large cavity which is likely a lipid binding pocket. About five percent of the mass of CP is acetone-extractable lipid, primarily the hydrophobic pigment astaxanthin (Fuller and Doolittle, 1971a).

The crustacean clot is formed by the transglutaminase-catalyzed crosslinking of lysine and glutamine sidechains (Fuller and Doolittle, 1971b). Two regions have been proposed as the likely crosslink sites on the basis of sequence comparisons: a 30-residue insert in the conserved amino-terminal β-barrel domain consisting mostly of threonine, serine, and lysine, and a glutamine-rich region in the carboxy-terminal portion of the molecule (Hall et al., 1999; Yeh et al., 1999). In micrographs of polymerized CP the molecules interact at localized points at the corners of CP dimers, the results of which would be very flexible polymers (Fuller and Doolittle, 1971b; Hall et al., 1999). Based on those micrographs, it is reasonable to suppose that the crosslink sites are at the vertices of the molecule as viewed at the top and bottom of Fig. 4A, and at the lower right and left in Fig. 4C.

While previous studies of CP by negative stain electron microscopy had not shown the large central cavity, its presence was not wholly unexpected. The crystal structure of lamprey vitellogenin, a homolog of CP, has a large funnel-shaped hydrophobic cavity in each half of the dimer which contains disordered phospholipids (Anderson et al., 1998). In the case of vitellogenin these pockets are offset, whereas in the CP structure the cavity forms a channel running directly through the molecule (Fig. 6). The cavity is most constricted at the surface, widening in the interior of the protein. A model has been proposed for the synthesis of the CP homolog apolipoprotein B in which lipids are added to the protein cotranslationally (Segrest et al., 1999). A similar possibility seems reasonable in the case of CP, in which lipids or pigment added cotranslationally would stabilize the large hydrophobic cavity.

The proposed lipid binding site that appears empty in cryoelectron micrographs and in the reconstructed volume is likely due to the lipid being less dense than the surrounding protein. A similar situation exists in the structure of the nicotinic acetylcholine receptor determined from cryoelectron micrographs, in which the lipid component does not appear in the final density (Unwin, 1993). The estimated volume of the cavity in the reconstructed volume is 75 nm^3, large enough to accommodate the expected number of astaxanthin molecules in a bilayer (Fig. 6).

The initial motivation to determine the structure of lobster CP by single particle reconstruction was to generate a model for low resolution phasing of crystal data. It has been possible, mostly with high symmetry particles such as viruses, to use EM reconstructions as molecular replacement models for generating initial phases at low resolution (see, for example, Dodson, 2001; Prasad et al., 1999; Rayment et al., 1982). Typically, molecular replacement solutions are found by searching an atomic model against the crystal data with the orientation and translation of the model determined separately (Rossmann and Blow, 1962). Recently, however, there has been some success with simultaneous six-dimensional rotation–translation searches with low resolution molecular envelopes (Liu et al., 2003). In the case of CP crystals the self rotation gave the orientation of the twofold dimeric axis, reducing the envelope search to four dimensions: a single rotation about the twofold noncrystallographic symmetry axis and three translational vectors. The solution with the lowest *R*-factor from an initial coarse search was improved by a finer six-dimensional search about that solution. This yielded a significant drop in the *R*-factor, indicative of a correct solution (Table 3).

The packing of CP dimers in the crystal unit cell is shown in Fig. 5. The measured overlap between symmetry related molecules is only 1.5% of the asymmetric unit volume. The lack of clashing in this solution is reassuring, especially because the molecular envelope search algorithm does not take crystal packing into account. Attempts are currently underway to extend phases generated from this search solution to the limit of the crystal data.

Acknowledgments

We thank Bridget Carragher and Clint Potter for helpful discussions about the reconstruction, Francisco Guerra for help with the computing, Jack Johnson for advice on the molecular envelope search, and Ed Kisfaludy for providing lobsters. J.M.K. is grateful to Russell Doolittle for his critical reading of the manuscript and for his enthusiastic support. Some of the work presented here was conducted at the National Resource for Automated Molecular Microscopy which is supported by the National Institutes of Health through the National Center for Research Resources' P41 Program (RR17573).

References

Anderson, T.A., Levitt, D.G., Banaszak, L.J., 1998. The structural basis of lipid interactions in lipovitellin, a soluble lipoprotein. Structure 15, 895–909.

Babin, P.J., Bogerd, J., Kooiman, F.P., Van Marrewijk, W.J., Van der Horst, D.J., 1999. Apolipophorin II/I, apolipoprotein B, vitellogenin, and microsomal triglyceride transfer protein genes are derived from a common ancestor. J. Mol. Evol. 49, 150–160.

Carragher, B., Kisseberth, N., Kriegman, D., Milligan, R.A., Potter, C.S., Pulokas, J., Reilein, A., 2000. Leginon: an automated system for acquisition of images from vitreous ice specimens. J. Struct. Biol. 132, 33–45.

Dodson, E.J., 2001. Using electron-microscopy images as a model for molecular replacement. Acta Crystallogr. D 57, 1405–1409.

Doolittle, R.F., Riley, M., 1990. The amino-terminal sequence of lobster fibrinogen reveals common ancestry with vitellogenins. Biochem. Biophys. Res. Commun. 167, 16–19.

Fuller, G.M., Doolittle, R.F., 1971a. Studies of invertebrate fibrinogen. I. Purification and characterization of fibrinogen from the spiny lobster. Biochemistry 10, 1305–1311.

Fuller, G.M., Doolittle, R.F., 1971b. Studies of invertebrate fibrinogen. II. Transformation of lobster fibrinogen into fibrin. Biochemistry 10, 1311–1315.

Hall, M., Wang, R., van Antwerpen, R., Sottrup-Jensen, L., Soderhall, K., 1999. The crayfish plasma clotting protein: a vitellogenin-related protein responsible for clot formation in crustacean blood. Proc. Natl. Acad. Sci. USA 96, 1965–1970.

Jones, T.A., Zou, J.Y., Cowan, S.W., Kjeldgaard, M., 1991. Improved methods for building protein models in electron density maps and the location of errors in these models. Acta Crystallogr. A 47, 110–119.

Kollman, J.M., Doolittle, R.F., 2005. Unusual non-crystallographic symmetry in crystals of a 420 kDa crustacean clottable protein. Acta Crystallogr. D 61, 485–489.

Kopacek, P., Hall, M., Soderhall, K., 1993. Characterization of a clotting protein, isolated from plasma of the freshwater crayfish *Pacifastacus leniusculus*. Eur. J. Biochem. 213, 591–597.

Liu, Q., Weaver, A.J., Xiang, T., Thiel, D.J., Hao, Q., 2003. Low-resolution molecular replacement using a six-dimensional search. Acta Crystallogr. D 59, 1016–1019.

Ludtke, S.J., Baldwin, P.R., Chiu, W., 1999. EMAN: semiautomated software for high-resolution single-particle reconstructions. J. Struct. Biol. 128, 82–97.

Otwinowski, Z., Minor, W., 1997. Processing of X-ray diffraction data collected in oscillation mode. Methods Enzymol. 276, 307–326.

Pettersen, E.F., Goddard, T.D., Huang, C.C., Couch, G.S., Greenblatt, D.M., Meng, E.C., Ferrin, T.E., 2004. UCSF chimera—a visualization system for exploratory research and analysis. J. Comput. Chem. 25, 1605–1612.

Potter, C.S., Chu, H., Frey, B., Green, C., Kisseberth, N., Madden, T.J., Miller, K.L., Nahrstedt, K., Pulokas, J., Reilein, A., Tcheng, D., Weber, D., Carragher, B., 1999. Leginon: a system for fully automated acquisition of 1000 electron micrographs a day. Ultramicroscopy 77, 153–161.

Prasad, B.V., Hardy, M.E., Dokland, T., Bella, J., Rossmann, M.G., Estes, M.K., 1999. X-ray crystallographic structure of the Norwalk virus capsid. Science 286, 287–290.

Raag, R., Appelt, K., Xuong, N.H., Banaszak, L., 1988. Structure of the lamprey yolk lipid-protein complex lipovitellin-phosvitin at 2.8 Å resolution. J. Mol. Biol. 200, 553–569.

Rayment, I., Baker, T.S., Caspar, D.L., Murakami, W.T., 1982. Polyoma virus capsid structure at 22.5 Å resolution. Nature 295, 110–115.

Richardson, P.E., Manchekar, M., Dashti, N., Jones, M.K., Beigneux, A., Young, S.G., Harvey, S.C., Segrest, J.P., 2005. Assembly of lipoprotein particles containing apolipoprotein-B: Structural model for the nascent lipoprotein particle. Biophys. J. (ePub ahead of print).

Rossmann, G.M., Blow, D.M., 1962. The detection of sub-units within the crystallographic asymmetric unit. Acta Crystallogr. D 15, 24–31.

Saxton, W.O., Baumeister, W., 1982. The correlation averaging of a regularly arranged bacterial cell envelope protein. J. Microsc. 127, 127–138.

Segrest, J.P., Jones, M.K., Dashti, N., 1999. N-terminal domain of apolipoprotein B has structural homology to lipovitellin and microsomal triglyceride transfer protein: a "lipid pocket" model for self-assembly of apob-containing lipoprotein particles. J. Lipid Res. 40, 1401–1416.

Schroeter, J.P., Bretaudiere, J.P., 1996. SUPRIM: easily modified image processing software. J. Struct. Biol. 116, 131–137.

Smolenaars, M.M., Kasperaitis, M.A., Richardson, P.E., Rodenburg, K.W., Van der Horst, D.J., 2005. Biosynthesis and secretion of insect lipoprotein: involvement of furin in cleavage of the apoB homolog, apolipophorin-II/I. J. Lipid. Res. 46, 412–421.

Soderhall, K., Cerenius, L., 1998. Role of the prophenoloxidase-activating system in invertebrate immunity. Curr. Opin. Immunol. 10, 23–28.

Unwin, N., 1993. Nicotinic acetylcholine receptor at 9 Å resolution. J. Mol. Biol. 20, 1101–1124.

Van Heel, M., 1987. Angular reconstitution: a posteriori assignment of projection directions for 3D reconstruction. Ultramicroscopy 21, 111–123.

Yeh, M.S., Huang, C.J., Leu, J.H., Lee, Y.C., Tsai, I.H., 1999. Molecular cloning and characterization of a hemolymph clottable protein from tiger shrimp (*Penaeus monodon*). Eur. J. Biochem. 266, 624–633.

Zhu, Y., Carragher, B., Potter, C., 2004. Contaminant detection: improving template matching based particle selection for cryo-electron microscopy. In: Proceedings of 2004 IEEE International Symposium on Biomedical Imaging, pp. 1071–1074.